Published in final edited form as:
Trends Biochem Sci. 2011 February ; 36(2): 117–125. doi:10.1016/j.tibs.2010.07.005.

Influence of Solubilizing Environments on Membrane Protein Structures

Timothy A. Cross[1,2,3,*], **Mukesh Sharma**[1,3], **Myunggi Yi**[2,4], and **Huan-Xiang Zhou**[2,4,*]

[1]Department of Chemistry and Biochemistry, Florida State University, Tallahassee, Florida, 32306

[2]Institute of Molecular Biophysics, Florida State University, Tallahassee, Florida, 32306

[3]National High Magnetic Field Laboratory, Florida State University, Tallahassee, Florida, 32306

[4]Department of Physics, Florida State University, Tallahassee, Florida, 32306

Abstract

Membrane protein structures are stabilized by weak interactions and are influenced by additional interactions with the solubilizing environment. Structures of Influenza virus A M2 protein, a proven drug target, have been determined in three different environments, thus providing a unique opportunity to assess environmental influences. Structures determined in detergents and detergent micelles can have notable differences from those determined in lipid bilayers. These differences make it imperative to validate membrane protein structures.

The importance of the membrane environment

Anfinsen's thermodynamic hypothesis [1] states “that the native conformation [of a protein] [SC1]is determined by the totality of inter-atomic interactions and hence by the amino acid sequence, in a given environment.” Too often these last four words are ignored. The influence of the environment on the structures of membrane proteins is especially significant (Box 1). Despite their functional importance, the structural biology of membrane proteins has been particularly challenging, as evidenced by the small number of membrane protein structures that have been determined (250 unique structures as of June, 2010; http://blanco.biomol.uci.edu/Membrane_Proteins_xtal.html). Integral membrane proteins are present in a heterogeneous environment that poses major obstacles for existing structural methodologies (Box 2). Hence one must contend with solubilizing membrane proteins in mimetics of the native membranes. However, it is very difficult to obtain membrane mimetic environments that support the native structure(s), dynamics, and function(s) of a membrane protein. In fact, functional assays of membrane proteins might not be feasible in the chosen membrane mimetic environment, as is the case for ion channels in detergent micelles. Consequently, adequate validation by functional assays has not been carried out for many membrane protein structures.

The influence of protein–membrane interactions compared to intra-protein interactions will be greater for smaller proteins and for proteins that do not have prosthetic groups to help

*Corresponding authors: Cross, T. A. (cross@magnet.fsu.edu) and Zhou, H.-X. (hzhou4@fsu.edu).

stabilize their transmembrane domains. In these cases, structural differences can be anticipated when characterizations are performed in different environments. Membrane proteins often have a degree of conformational plasticity distinguishing them from water-soluble proteins. This plasticity might be required for their function under native conditions, such as for a protein that cycles through closed, activated, open, and inhibited states. So the task of structural biology for a membrane protein is not only to determine a structure, but rather the native structures in all functional states in order to construct mechanistic models.

The main aim of the present review is to compare the structures of the Influenza A virus M2 protein determined from samples in liquid crystalline lipid bilayers, samples crystallized from detergents, and samples in detergent micelles (Box 2). It is clear that the membrane mimetic environments have significant influence on the M2 structures. Although the structural differences of the various samples reflect the conformational plasticity of the protein, it is not clear that they are all relevant to the protein's function under native conditions. Indeed, some of the structures have features that are not compatible with the protein's proton conductance activity. By contrast, different structural methodologies, while specializing in different membrane mimetic environments, provide complementary data, which together can facilitate structural characterization of the functional states. Data obtained from lipid bilayers have a unique role in characterizing the native structures of membrane proteins and validating structures determined in other membrane mimetic environments.

The Influenza virus A M2 proton channel

The M2 protein functions as a homotetramer; each monomer, consisting of 97 residues has a single transmembrane (TM) helix [2]. M2 has three independent functional domains. The N-terminal 24 residues form a viral budding domain [3]. The TM helix (residues 25-46), along with a membrane surface-bound amphipathic helix (residues 47-62), forms the proton conductance domain that adequately reproduces the conductance properties of full-length protein [4, 5]. Finally, the C-terminal domain (residues 63-97) binds the M1 protein, promoting viral assembly [6].

Ion transport through M2 is highly proton selective and activated by low pH in the viral exterior [7-10]. Although this protein has long been called a channel, the consensus conductance rate now suggests that proton transport is mediated by an internal binding site [11-16]. In liposome assays, typically used for transporters, the reconstituted full-length protein [5, 9, 17], the TM domain [5, 14], and the conductance domain [5] appear to have robust activity and excellent sensitivity to a channel-blocking drug, amantadine. Truncation reduces the tetramer stability at low pH [18], more so for the TM domain than for the conductance domain [19]. Reduction in tetramer stability leads to reduced proton conductance and drug efficacy [5].

Until recently, amantadine and a derivative, rimantadine, were effective in blocking the proton conducting function of the M2 protein, leading to cessation of viral replication [20, 21]. However, the widespread occurrence of the S31N mutation in the H3N2 and H1N1 viral strains [22, 23] has resulted in drug resistance in the past few flu seasons and in the recent swine flu pandemic. As with the strong interest in new inhibitors of hemagglutinin, another Influenza coat protein [24], detailed knowledge of the structure(s), dynamics, and functions of the M2 protein should lead to enhanced opportunities for drug development.

Comparison of M2 structures

A model of the TM domain was built from cross-linking data that correctly identified residues facing the pore and the tetrameric state of the functional protein [12]. Since then,

solid-state NMR spectroscopy, X-ray crystallography, and solution NMR spectroscopy (Box 2) have all been applied for M2 structure determination. Thus the M2 protein provides the only example where structures have been determined in three different environments from three key methodologies. A comparison of these structures therefore provides great insight into the influence of membrane mimetic environments.

Solid-state NMR structures

In 2002 the first backbone structure of the M2 TM domain (residues 22-46) was determined using high-precision orientational restraints from solid-state NMR spectroscopy of uniformly aligned bilayer samples and distance restraints from magic angle spinning (MAS) spectroscopy of liposome samples (PDB entry 1NYJ; Figure 1a) [25]. This provided details of the helical backbone structure including a precise characterization of the substantial helical tilt (~35°), the helical rotation, and the left-handed packing of the tetrameric bundle of helices in lipid bilayers [26]. A single labeled site in these samples always generated a single resonance, indicating structural homogeneity and four-fold symmetry on the ms to sub-ms timescale. The substantial helical tilt resulted in a cavity in the N-terminal pore that appeared to be appropriate for amantadine binding. The sample preparation involved organic solvent cosolubilization of peptide and lipid followed by drying and rehydration to form aligned bilayers. A later protocol [18] involved the formation of buffered liposomes followed by preparation of aligned samples. This latter preparation showed evidence of more backbone dynamics, some conformational heterogeneity, and a slightly reduced helical tilt of 32° [18]. Nevertheless the M2 TM domain is much more stable in a lipid bilayer than in a detergent micelle [27].

The heart of the mechanism for M2 acid activation and proton conductance is the His37 tetrad [11-16]. Solid evidence for the role of His37 in acid activation was provided by the loss of pH dependence in proton conductance by His37 substitutions [11, 13]. His37 has also been specifically proposed to be the obligatory binding site for the permeant proton [12, 15, 16]. Furthermore, the pKas of the His37 tetrad (one residue from each monomer in this tetrameric protein) were determined in liposomes using MAS NMR [14]. The pKas for binding the first two protons were both 8.2, indicating high proton affinity and cooperative binding. Chemical shift data further showed that each of the two protons is shared between a pair of His37 imidazoles, resulting in two strong hydrogen bonds to form a “histidine-locked” state. Binding of the third proton, with pKa = 6.3, activates the channel by breaking the histidine-locked state. His37 and Trp41 can form cation-π interactions [28]; so the tetrameric cluster of His37 and Trp41 functions as a unit, which we refer to as the HxxxW quartet. A short distance observed between Trp C_{γ} and His $N_{\delta 1}$ supports this contention (Figure 1a) [25].

In 2007 the backbone structure of the M2 TM domain in the presence of amantadine was determined using orientational restraints, again in aligned lipid bilayers, but this time using the liposome protocol (PDB entry 2H95; Figure 1b) [29]. The spectral resonances implied four-fold symmetry and far less structural heterogeneity and dynamics, suggesting that the drug substantially stabilized the structure [18]. This structure showed a kink in the TM helices near Gly34 such that the N-terminal segment of the TM helix retains a very similar tilt angle to that of the apo form, while the C-terminal segment has a tilt angle reduced to ~20°.

Molecular dynamics simulations [30] starting from the structures in the absence and presence of amantadine provided additional insight into proton transport and drug binding in the pore. The Val27 residues near the pore entrance transiently broke the water wire through the pore (Figure 1c&d), leading to the proposition of a secondary gate in addition to the primary gate formed by Trp41 [10]. Besides limiting the proton flux, the Val27 gate also

limits the binding rate constant of amantadine and assists the bound amantadine by forming an extended blockage (Figure 1c&d). The bound amantadine is quite dynamic, but predominantly interacts with Ala30 and Ser31 and has a time averaged orientation with its C–N vector toward the M2 C-terminus. The position and orientation from the simulations are confirmed by a recent structural refinement, using the NMR data of Hu et al. [29] supplemented by distance restraints between the drug molecule and the TM domain [31]. The interactions of bound amantadine with Ala30 and Ser31 explain why a number of mutations, including S31N, at these positions lead to drug resistance.

Interestingly, amantadine binding dramatically downshifts the pKas of the His37 tetrad and prevents the formation of strong imidazole–imidazolium hydrogen bonds [32]. The perturbation on the chemistry of the His37 tetrad suggests an alternative to steric blockage or conformational rigidification as possible mechanisms for the inhibitory action of amantadine.

To correlate function with structure and dynamics, a proton transport model was proposed, in which the proton flux is determined by the rate constants for binding to the His37 tetrad from the N-terminal and C-terminal sides and the corresponding rate constants for unbinding [15, 16]. The model predicts that the proton flux saturates at low pH on the N-terminal side and the transition occurs around the third pKa of the His37 tetrad. These predictions are supported by conductance measurements [7]. The low conductance rate of M2 [9, 17] is further explained by the dynamics of the Trp41 primary gate and the Val27 secondary gate [16].

Crystal structures

Two crystal structures of the TM domain and one solution NMR structure of the conductance domain were published in 2008 [33, 34]. The crystals were formed in octylglucoside solutions. One of the crystal structures was obtained at neutral pH at 2.05 Å resolution (PDB entry 3BKD) and the other (actually a G34A mutant) at pH 5.3 with amantadine bound at 3.5 Å resolution (PDB entry 3C9J) (Figure 2). Both crystal structures show a left-handed tetrameric bundle of TM helices with hydrophilic residues facing the pore as in earlier structures [25, 29]. The tilt of the TM helices in these structures is similar to that seen in the bilayer structures [25, 29]. One of the helices of the neutral-pH structure showed a significant kink, as seen in the bilayer amantadine-bound structure [15, 29, 31]. Today, the G34A structure remains the only structure determined at low pH. It should be noted that Gly34 is the site at which the helix kinks in response to amantadine binding and for its conductance mechanism. Therefore, decreasing the torsion space available to this residue by substituting alanine for glycine might interfere with structural, dynamical, and functional characteristics. With this mutation, the M2 conductance is reduced by 60% [35].

Significantly, the neutral-pH structure has splayed helices; consequently the crossing point for the helices shifted dramatically toward the N-terminus (Figure 4a), thereby preventing the formation of a pore that is contained by the four-helix bundle (Figure 2c). Although lipids are known to be integral components of some membrane protein complexes [36], here octylglucoside and polyethylene glycol occupy space between 3 of the 4 helical interfaces as well as the C–terminal pore (Figure 2d). The helical interface that is not perturbed by octylglucoside or polyethylene glycol appears to be similar to the helical interfaces observed in the lipid-bilayer structures [25, 29]. The octylglucoside headgroups actually interact with the functionally critical His37 and Trp41 sidechains. In addition, there is a large contact surface area between the two tetramers that make up the unit cell (Figure 2e). The substantial crystal contacts could influence the tetramer structure, which is only stabilized by weak interactions due to the amino acid composition of the TM domain. These influences might suggest non-native like conformations or they might suggest a range of

conformational states that are accessible to the protein in native membranes. Although functional assays in liposomes [5, 14] document the conductance activity of the construct, they do not validate the structure obtained from a detergent environment. Agreement with the helical tilt observed in lipid bilayers is a significant step toward validation, but still the helix crossing point is very different (Figure 4).

Solution NMR structures

DHPC (1,2 dihexanoyl-*sn*-glycerophosphocholine) micelles were used for solubilization in the solution NMR structure determination [33]. To overcome the low stability of the TM domain in detergent micelles, this structural determination was performed on a larger construct (residues 18-60), the conductance domain, at neutral pH (PDB entry 2RLF). Again, a left-handed tetrameric helical bundle was observed with hydrophilic residues in the interior and the pore is well enclosed by the helical bundle. However, this structure proved to be controversial in three respects. First, the drug binding site was observed on the outside of the TM tetrameric bundle with a stoichiometry of 4 drugs per tetramer (Figure 3). Second, the TM helices are nearly parallel to each other resulting in tight packing of the helices that prevents the formation of an N-terminal cavity large enough for drug binding in the pore. Furthermore, the tight packing of the helices might hinder the Trp41 indoles from forming strong interactions with the histidine tetrad. Third, the amphipathic helix (residues 50-60) formed a water-soluble bundle with a hydrophobic core, tethered flexibly to the TM domain by residues 47-49 that were not observed due to considerable dynamics. In a lipid bilayer this structure would position the amphipathic helical bundle in the bulk aqueous environment.

Although helices that are longer than the thickness of a lipid bilayer are frequently constrained to tilt in the bilayer [37, 38], the hydrophobic dimension of a detergent micelle (Box 3) can expand to match the length of the hydrophobic surface of a helix [39, 40]. This feature of a micelle environment results in a helical bundle with nearly parallel helices potentially preventing drug binding in the pore and proper functioning of the HxxxW quartet. Recent distance measurements between the drug and the TM domain in a lipid bilayer demonstrate that the primary binding site is in the pore (consistent with previous experimental data and molecular dynamics simulations [30, 32]), although there also appears to be a weak binding site on the tetramer exterior [31]. Studies of the TM domain confirmed that the primary binding site is in the pore, with a stoichiometry of one drug per tetramer [41]. That the amphipathic helix appears as a water-exposed bundle could also be a result of detergent solubilization. In bilayer samples of the full-length protein [42] and of the conductance domain [43] this helix is positioned in the lipid interface. Such a position for the amphipathic helix might also interfere with the exterior drug binding site.

Cautionary note on the use of detergents for solubilization

Several differences between lipids and detergents potentially influence protein structures (Box 3). First, there is typically a mM concentration of monomeric detergents present, whereas monomeric lipid concentrations are many orders of magnitude lower [44]. Indeed, in the M2 crystal structures, monomeric detergents penetrate into the aqueous pore of the TM domain appearing to compromise the protein's functionality.

Secondly, the hydrophobic dimension of detergent micelles is readily expandable [39, 40], and consequently helices designed to have a hydrophobic mismatch for inducing helical tilt in a membrane can be packed tightly together. This appears to be the situation for the helical bundle characterized by solution NMR, in which the HxxxW functionality is probably disrupted.

Thirdly, in comparison with the planar surface of a membrane, the high degree of curvature for a micellar surface might interfere with the surface binding of amphipathic helices [45-47]. The solution NMR structure of the conductance domain in micelles has the amphipathic helix solubilized in the bulk aqueous solution, in contrast to results in lipid bilayers [42, 43].

Fundamentally, the interactions that stabilize the quaternary structure of M2 are weak and relatively non-specific. Cartoons of three M2 TM structures (Fig. 4) illustrate that the protein's environment affects the delicate balance of interactions governing helix packing. It is anticipated that the conformations associated with different functional states will utilize different helix packing, helix kinking, as well as differences in sidechain rotamers. To what extent the native conformational states are captured by the structures in different environments described here is still to be ascertained.

Environmental influences on other membrane protein structures

There are many examples in the literature of structures that experience dramatic influences by the membrane mimetic environment, including those of KvaP, KCNE1, Smr, and Phospholamban [48-51]. There are probably many other examples with more subtle influences that have not been identified, because there is relatively little structural data for membrane proteins obtained from bilayer environments for validating these structures.

Many of the successful membrane protein structures in the PDB are characterized by X-ray crystallography and are very large structures in which it can be anticipated that the interactions with the membrane mimetic environments are small in comparison to those within the protein structures. Many more membrane proteins, such as the electron transport proteins, have prosthetic groups in the TM domains that could serve to stabilize tertiary and quaternary structures of these domains. However, for many prokaryotic membrane proteins, where the number of TM helices is small, the interactions with the environment could become significant. Of the 1100 predicted α-helical integral membrane proteins from the *Mycobacterium tuberculosis* genome, nearly 60% of these proteins are predicted to contain 1, 2, or 3 putative TM helices [52]. Even taking into account that many of these proteins are oligomeric, a great many membrane proteins are predicted to have relatively small TM domains. Such small domains are particularly sensitive to the influence of membrane mimetic environments, potentially leading to non-native structures; larger domains might also be influenced by these environments.

Concluding remarks

Fortunately, there are many sample preparation conditions that can be chosen for crystallization and for solution NMR. Detergents represent a diverse set of compounds with an equally diverse morphology [53, 54]. Consequently, screening of sample conditions might lead to conditions that support native-like structures. Indeed, a new crystal structure of the M2 TM domain (PDB entry 3LBW) has been determined that is not only largely consistent with the solid-state NMR derived orientational restraints but also has a helix crossing point near the bilayer center and a pore contained by the TM helical bundle (W. DeGrado, personal communication). Although the hazards of using detergents as membrane mimetics have been emphasized here, artificial lipid bilayers also represent a mimetic of the native membrane environment and hence structures determined in synthetic bilayers might not reflect the exact native structure. For instance, the helical tilt in M2 TM is dependent on the fatty acyl chain length of synthetic bilayers [37]. This emphasizes that all membrane protein structural biology should be subjected to careful scrutiny and through a combination of structural methodologies it should be possible to achieve an understanding of the native functional state.

Membrane proteins represent a major challenge for structural biology. Not only are these structures more dynamic, having greater conformational plasticity through which the proteins function, but their structures are significantly influenced by their environments, reminiscent of the words in Anfinsen's thermodynamic hypothesis [1]. It is, therefore, not enough to show that a protein construct is functional to validate a structure, unless the functional assay is performed in the same environment as that used for the structural characterization. Structural data obtained in an appropriate lipid bilayer environment can serve as benchmarks for validating structures determined in other mimetic environments. It is exciting that a variety of structural methods including solid-state NMR, electron spin resonance, and cryo-electron microscopy are now providing an increasing quantity of structural data for membrane proteins in bilayer environments.

Box 1

Transmembrane vs. water-soluble proteins

Transmembrane α-helices have an increased composition of hydrophobic amino acid residues and a vastly decreased content of charged and highly polar residues (Figure I) [55]. The reduced potential to form site-specific electrostatic and hydrogen bonding interactions between helices leaves van der Waals interactions as the dominant source of stability for tertiary and quaternary structure in the transmembrane region. The resulting modest tertiary and quaternary stability facilitates structural rearrangements necessary for functional mechanisms.

A fundamental result of the increased hydrophobic nature of the transmembrane domain is the protection of polar sites, both in the sidechains and in the backbone. For the backbone, the typical torsion angles for TM α-helices differ from those of water-soluble helices (ϕ/ψ of −60°/−45° vs. −65°/−40°, respectively) [56, 57]. Consequently, the carbonyl oxygen does not project outward from the helix axis as much in TM helices, thereby shielding the substantial partial charge on these sites and strengthening the intra-helical hydrogen bonds [56].

Serine and threonine are the two polar residues that have increased occurrence in the TM helices (Figure I) [55]. Both residues have the potential to hydrogen bond, through their hydroxyl groups, to their helical backbone. Such intra-helical hydrogen bonding allows the polar sidechains to be sequestered in a hydrophobic environment, thus facilitating initial helical insertion into the membrane. Once in the membrane, these polar sidechains can form inter-helical hydrogen bonds [58]. Interestingly, glycine and proline, known as helix breakers in water-soluble proteins, are well integrated into TM helices. Given their propensity to drive helix kinking, these residues are referred to as pro-kink sites in TM helices [57]; helix kinking can play central roles in functional mechanisms [15, 59, 60].

Importantly, the largely hydrophobic sidechain composition in TM domains results in a relatively sterile chemical environment. The presence of serine and threonine residues helps to ameliorate this condition, as do imperfections in the uniformity of the helical structure. Prolines result in an exposed carbonyl oxygen without a hydrogen bonding partner. Similarly, helical kinks and π-bulges expose amide protons and carbonyl oxygens as potential sites for inter-helical interactions and chemical reactivity. Consequently, structural knowledge of TM helices are critical for functional understanding of membrane proteins.

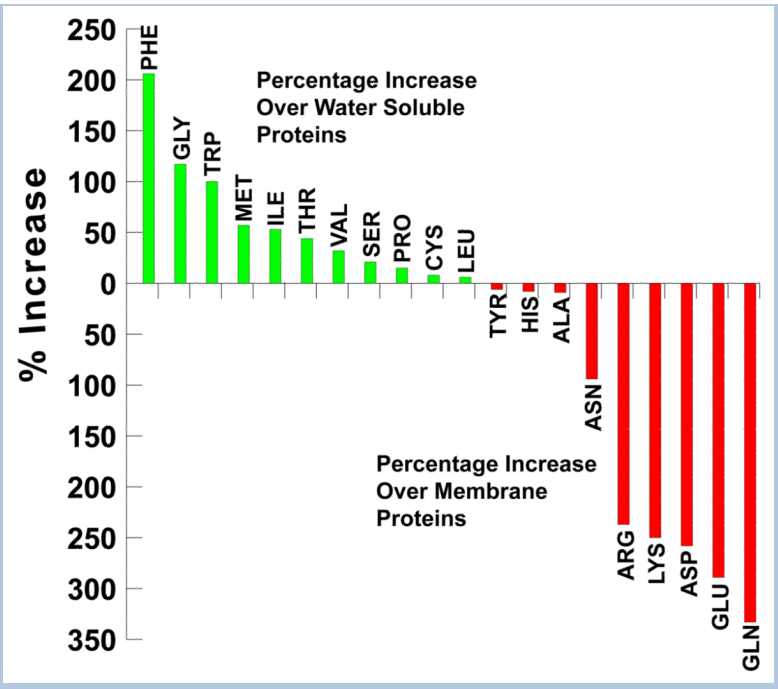

Figure I.
Comparison of amino acid compositions between water-soluble protein helices and transmembrane protein helices. In green and red are amino acids which are more common in membrane protein TM helices and in water-soluble protein helices, respectively. Adapted from ref. [79] with permission; copyright (2007) John Wiley & Sons, Inc.

Box 2

Methodologies for structural determination of membrane proteins

All of the structural methodologies for membrane proteins require solubilization of the proteins in environments that model native membranes. Crystallization for X-ray diffraction requires high protein concentration and dominant specific interactions at the unit cell interface. These are typically polar and charge–charge interactions and hence hydrophobic membrane-soluble surfaces are normally shielded from the unit cell boundaries. Similarly, the hydrophobic interstices of lipid bilayers cannot span between crystalline unit cells. Most often, detergents are used to achieve high solubility of membrane proteins and to shield the hydrophobic surface of the protein. However, it has frequently been noted that lipids are essential for the formation of quality crystals [61-63], and non-traditional methods of crystallization facilitated by the use of bicelles or lipidic cubic phases have occasionally been used to generate good crystals [64, 65]. In addition to manipulating the environment for protein crystallization, the protein itself is often modified by mutations, truncations, and/or through the formation of fusion proteins to achieve crystallization [48, 66, 67].

Solution NMR requires that the protein tumbles isotropically on the NMR timescale; otherwise, the spectral resolution will be lost. The molecular weight for the tetrameric M2 conductance domain is already 22 kDa; therefore the molecular weight added by detergents must be minimized to avoid a significant increase in the global correlation time. Consequently, small detergent micelles are favored, as are micelles within which

the protein has more mobility [68]. However, detergent micelles have numerous features that distinguish them from a lipid bilayer (Box 3). Recently, small bicelle structures prepared from a mixture of lipids and detergents have been used [69, 70], and these might prove to be a better membrane mimetic environment.

Solid-state NMR of uniformly aligned samples utilizes liquid crystalline planar lipid bilayers as a membrane mimetic. Synthetic bilayers can reproduce many of the characteristics of the native membrane. Gradients in dielectric constant, water concentration, fluidity and even the lateral pressure profile across the native membrane can be modeled in synthetic bilayers. The lipid composition can be crudely reproduced, but the asymmetries of the bilayer are not modeled, such as the differing lipid composition in the outer and inner leaflets and the various electrical, chemical, and mechanical gradients across the bilayer.

Box 3

Modeling the native membrane

Cellular membranes host a broad spectrum of essential and complex functions. They maintain electrical, mechanical, and chemical gradients as well as structural integrity during events such as cell division and endocytosis. Consequently, membranes have a high concentration of proteins packed into these critical cellular surfaces and interfaces [71]. The lipid composition in both leaflets of the bilayer is complex and unique, comprising more than 100 different lipids. Membranes can also be heterogeneous, with some regions having high concentrations of cholesterol and sphingomyelin [72]. These complexities are required for the broad range of tasks performed by membranes.

The heterogeneous environment of native membranes is not compatible with atomic resolution structural characterization; consequently the membrane is modeled to mimic the native condition. Lipids have complex phase diagrams as a function of concentration, composition, and temperature. Dynamics in the fatty acyl region can lead to gel and liquid crystalline phases, but hexagonal and cubic phases have much more curvature [73]. Native planar membranes at biological temperatures often exist near the phase boundaries where considerable distortions of the bilayer facilitate processes such as cell division and membrane fusion. However, lipid bilayers form structures with relatively well-defined hydrophobic dimensions. In addition, lipid bilayers have a dramatic lateral pressure profile [74], a substantial interfacial region between bulk water and an almost completely dehydrated hydrocarbon interior [75, 76]. Consequently, there is a dramatic water concentration gradient, a dynamics gradient from the lipid backbone region to the center of the bilayer, and dielectric constant gradient from 80 in the bulk aqueous environment, to 200 in the headgroup region [77], to 2 in the bilayer interstices.

Detergents also have complex phase diagrams, including a monomeric phase. Above a certain total concentration, known as the critical micelle concentration (CMC), the monomeric concentration is essentially equal to the CMC [39]. The CMC is typically mM and thus orders of magnitude above lipid monomeric concentrations [44]. Detergents form monolayers, not bilayers. Although monolayers can fold back on themselves to give the appearance of a bilayer, they have a single hydrophilic surface, unlike bilayers which have two separate hydrophilic surfaces. Micelles do not have a well-defined hydrophobic dimension; indeed it can expand to conform to the hydrophobic dimension of a peptide (Figure I) or protein [39, 40]. In addition, pro-kink (Box 1) sites in the middle of a TM helix can seek the hydrophilic surface without requiring the hydrophilic N- or C-termini to migrate across the hydrophobic interstices. This is not true for bilayers. Detergent

micelles also have a much greater surface curvature, a less dramatic dielectric constant and water concentration gradients.

The amino acid composition of membrane proteins is engineered to minimize potential electrostatic interactions; backbone hydrogen bonding capacity is almost completely fulfilled through secondary structure formation. Electrostatic interactions are dependent on the dielectric constant, hydrophobic interactions require the presence of water, and water, when present, is a catalyst for hydrogen bond exchange – all of these factors are different in the various membrane mimetic environments.

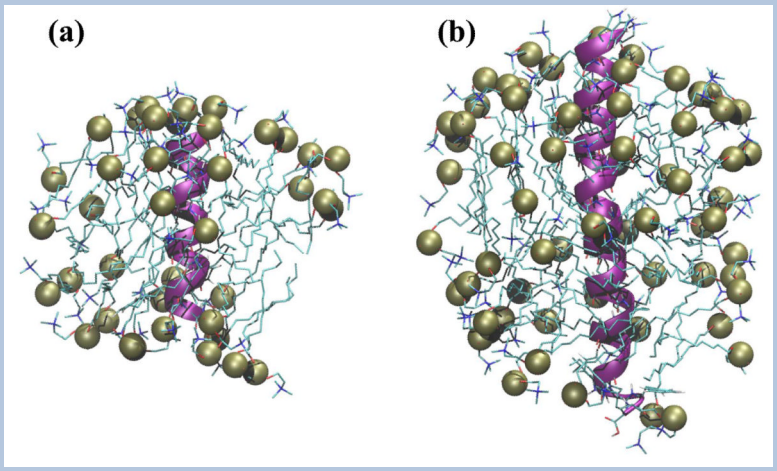

Figure I.

Solubilization of two helical peptides with different lengths in dodecylphosphocholine (DPC) micelles. (**a**) WALP16, with the sequence $GWW(LA)_5WWA$. (**b**) WALP35, with the sequence $GWW(LA)_{14}LWWA$. The two peptides were solvated in a 40-DPC micelle surrounded by 5000 water molecules, and in a 65-DPC micelle surrounded by 8125 water molecules, respectively. Shown are snapshots after ~10 ns of molecular dynamics simulations under constant temperature (300 K) and constant pressure (1 bar). The peptides are shown as ribbons; phosphorus atoms of the DPC molecules are shown as spheres. Note the exposure of some DPC hydrocarbon tails to the aqueous environment.

Acknowledgments

This work was supported in part by National Institutes of Health Grant AI23007. Some of the research was conducted at the National High Magnetic Field Laboratory supported by Cooperative Agreement 0654118 between the Division of Materials Research, National Science Foundation and the State of Florida.

References

1. Anfinsen CB. Principles that govern the folding of protein chains. Science. 1973; 181:223–230. [PubMed: 4124164]
2. Pinto LH, Lamb RA. Controlling influenza virus replication by inhibiting its proton channel. Mol. Biosyst. 2007; 3:18–23. [PubMed: 17216051]
3. Park EK, et al. The M2 ectodomain is important for its incorporation into influenza A virions. J. Virol. 1998; 72:2449–2455. [PubMed: 9499106]
4. Tobler K, et al. Effect of cytoplasmic tail truncations on the activity of the M(2) ion channel of influenza A virus. J Virol. 1999; 73:9695–9701. [PubMed: 10559278]
5. Ma C, et al. Identification of the functional core of the influenza A virus A/M2 proton-selective ion channel. Proc. Natl. Acad. Sci. USA. 2009; 106:12283–12288. [PubMed: 19590009]

6. Chen BJ, et al. The influenza virus M2 protein cytoplasmic tail interacts with the M1 protein and influences virus assembly at the site of virus budding. J. Virol. 2008; 82:10059–10070. [PubMed: 18701586]
7. Chizhmakov IV, et al. Selective proton permeability and pH regulation of the influenza virus M2 channel expressed in mouse erythroleukaemia cells. J. Physiol. 1996; 494(Pt 2):329–336. [PubMed: 8841994]
8. Mould JA, et al. Mechanism for proton conduction of the M2 Ion Channel of Influenza A Virus. J. Biol. Chem. 2000; 275:8592–8599. [PubMed: 10722698]
9. Lin TI, Schroeder C. Definitive assignment of proton selectivity and attoampere unitary current to the M2 ion channel protein of influenza A virus. J. Virol. 2001; 75:3647–3656. [PubMed: 11264354]
10. Tang Y, et al. The gate of the influenza virus M2 proton channel is formed by a single tryptophan residue. J. Biol. Chem. 2002; 277:39880–39886. [PubMed: 12183461]
11. Wang C, et al. Activation of the M2 ion channel of influenza virus: a role for the transmembrane domain histidine residue. Biophys. J. 1995; 69:1363–1371. [PubMed: 8534806]
12. Pinto LH, et al. A functionally defined model for the M2 proton channel of influenza A virus suggests a mechanism for its ion selectivity. Proc. Natl. Acad. Sci. USA. 1997; 94:11301–11306. [PubMed: 9326604]
13. Venkataraman P, et al. Chemical rescue of histidine selectivity filter mutants of the M2 ion channel of influenza A virus. J. Biol. Chem. 2005; 280:21463–21472. [PubMed: 15784624]
14. Hu J, et al. Histidines, heart of the hydrogen ion channel from influenza A virus: toward an understanding of conductance and proton selectivity. Proc Natl Acad Sci U S A. 2006; 103:6865–6870. [PubMed: 16632600]
15. Yi M, et al. Conformational heterogeneity of the M2 proton channel and a structural model for channel activation. Proc. Natl. Acad. Sci. USA. 2009; 106:13311–13316. [PubMed: 19633188]
16. Zhou HX. Diffusion-influenced transport of ions across a transmembrane channel with an internal binding site. J. Phys. Chem. Lett. 2010; 1:1973–1976. [PubMed: 20625440]
17. Moffat JC, et al. Proton transport through influenza A virus M2 protein reconstituted in vesicles. Biophys. J. 2008; 94:434–445. [PubMed: 17827230]
18. Li C, et al. Solid-state NMR characterization of conformational plasticity within the transmembrane domain of the influenza A M2 proton channel. Biochim. Biophys. Acta. 2007; 1768:3162–3170. [PubMed: 17936720]
19. Salom D, et al. pH-dependent tetramerization and amantadine binding of the transmembrane helix of M2 from the influenza A virus. Biochemistry. 2000; 39:14160–14170. [PubMed: 11087364]
20. Grambas S, et al. Influence of amantadine resistance mutations on the pH regulatory function of the M2 protein of influenza A viruses. Virology. 1992; 191:541–549. [PubMed: 1448912]
21. Lamb RA, et al. Influenza virus M2 protein is an integral membrane protein expressed on the infected-cell surface. Cell. 1985; 40:627–633. [PubMed: 3882238]
22. Hayden FG. Antiviral resistance in influenza viruses--implications for management and pandemic response. N. Engl. J. Med. 2006; 354:785–788. [PubMed: 16495389]
23. Gubareva L, et al. Update: Drug Susceptibility of Swine-Origin Influenza A (H1N1) Viruses, April 2009. Morbidity Mortality Weekly Rep. 2009; 58:1–3.
24. Skehel JJ, Wiley DC. Receptor binding and membrane fusion in virus entry: the influenza hemagglutinin. Annu Rev Biochem. 2000; 69:531–569. [PubMed: 10966468]
25. Nishimura K, et al. The closed state of a H+ channel helical bundle combining precise orientational and distance restraints from solid state NMR. Biochemistry. 2002; 41:13170–13177. [PubMed: 12403618]
26. Wang J, et al. Structure of the transmembrane region of the M2 protein H^+ channel. Protein Sci. 2001; 10:2241–2250. [PubMed: 11604531]
27. Cristian L, et al. Use of thiol-disulfide equilibria to measure the energetics of assembly of transmembrane helices in phospholipid bilayers. Proc. Natl. Acad. Sci. USA. 2003; 100:14772–14777. [PubMed: 14657351]

28. Okada A, et al. Protonation of histidine and histidine-tryptophan interaction in the activation of the M2 ion channel from influenza a virus. Biochemistry. 2001; 40:6053–6060. [PubMed: 11352741]
29. Hu J, et al. Backbone structure of the amantadine-blocked trans-membrane domain M2 proton channel from Influenza A virus. Biophys. J. 2007; 92:4335–4343. [PubMed: 17384070]
30. Yi M, et al. A secondary gate as a mechanism for inhibition of the M2 proton channel by amantadine. J. Phys. Chem. B. 2008; 112:7977–7979. [PubMed: 18476738]
31. Cady SD, et al. Structure of the amantadine binding site of influenza M2 proton channels in lipid bilayers. Nature. 2010; 463:689–692. [PubMed: 20130653]
32. Hu , et al. The chemical and dynamical influence of the anti-viral drug amantadine on the M2 proton channel transmembrane domain. Biophys. J. 2007; 93:276–283. [PubMed: 17434944]
33. Schnell JR, Chou JJ. Structure and Mechanism of the M2 Proton Channel of Influenza A Virus. Nature. 2008; 451:591–595. [PubMed: 18235503]
34. Stouffer AL, et al. Structural basis for the function and inhibition of an influenza virus proton channel. Nature. 2008; 451:596–599. [PubMed: 18235504]
35. Balannik V, et al. Functional studies and modeling of pore-lining residue mutants of the influenza a virus M2 ion channel. Biochemistry. 2010; 49:696–708. [PubMed: 20028125]
36. Palsdottir H, Hunte C. Lipids in membrane protein structures. Biochim. Biophys. Acta. 2004; 1666:2–18. [PubMed: 15519305]
37. Duong-Ly KC, et al. The conformation of the pore region of the M2 proton channel depends on lipid bilayer environment. Protein Sci. 2005; 14:856–861. [PubMed: 15741338]
38. Nyholm TK, et al. How protein transmembrane segments sense the lipid environment. Biochemistry. 2007; 46:1457–1465. [PubMed: 17279611]
39. Garavito RM, Ferguson-Miller S. Detergents as tools in membrane biochemistry. J. Biol. Chem. 2001; 276:32403–32406. [PubMed: 11432878]
40. Fernandez C, et al. Lipid-protein interactions in DHPC micelles containing the integral membrane protein OmpX investigated by NMR spectroscopy. Proc. Natl. Acad. Sci. USA. 2002; 99:13533–13537. [PubMed: 12370417]
41. Sharma M, et al. Drug sensitivity, drug-resistant mutations, and structures of the conductance domains of three viral porins. BBA-Biomembranes. 2010 in press.
42. Tian C, et al. Initial structural and dynamic characterization of the M2 protein transmembrane and amphipathic helices in lipid bilayers. Protein Sci. 2003; 12:2597–2605. [PubMed: 14573870]
43. Nguyen PA, et al. pH-induced conformational change of the influenza M2 protein C-terminal domain. Biochemistry. 2008; 47:9934–9936. [PubMed: 18754675]
44. Cevc, G.; Marsh, D. Phospholipid Bilayers: Physical Principles and Models. Wiley; 1987.
45. Choowongkomon K, et al. A structural model for the membrane-bound form of the juxtamembrane domain of the epidermal growth factor receptor. J. Biol. Chem. 2005; 280:24043–24052. [PubMed: 15840573]
46. Chou JJ, et al. Micelle-induced curvature in a water-insoluble HIV-1 Env peptide revealed by NMR dipolar coupling measurement in stretched polyacrylamide gel. J. Am. Chem. Soc. 2002; 124:2450–2451. [PubMed: 11890789]
47. Traaseth NJ, et al. Spectroscopic validation of the pentameric structure of phospholamban. Proc Natl Acad Sci U S A. 2007; 104:14676–14681. [PubMed: 17804809]
48. Lee SY, et al. Structure of the KvAP voltage-dependent K+ channel and its dependence on the lipid membrane. Proc Natl Acad Sci U S A. 2005; 102:15441–15446. [PubMed: 16223877]
49. Poget SF, Girvin ME. Solution NMR of membrane proteins in bilayer mimics: small is beautiful, but sometimes bigger is better. Biochim Biophys Acta. 2007; 1768:3098–3106. [PubMed: 17961504]
50. Oxenoid K, Chou JJ. The structure of phospholamban pentamer reveals a channel-like architecture in membranes. Proc Natl Acad Sci U S A. 2005; 102:10870–10875. [PubMed: 16043693]
51. Kang C, et al. Structure of KCNE1 and implications for how it modulates the KCNQ1 potassium channel. Biochemistry. 2008; 47:7999–8006. [PubMed: 18611041]

52. Korepanova A, et al. Cloning and expression of multiple integral membrane proteins from Mycobacterium tuberculosis in Escherichia coli. Protein Sci. 2005; 14:148–158. [PubMed: 15608119]
53. Columbus L, et al. Mixing and matching detergents for membrane protein NMR structure determination. J Am Chem Soc. 2009; 131:7320–7326. [PubMed: 19425578]
54. Lipfert J, et al. Size and shape of detergent micelles determined by small-angle X-ray scattering. J Phys Chem B. 2007; 111:12427–12438. [PubMed: 17924686]
55. Eilers M, et al. Comparison of helix interactions in membrane and soluble alpha-bundle proteins. Biophys. J. 2002; 82:2720–2736. [PubMed: 11964258]
56. Kim S, Cross TA. Uniformity, ideality, and hydrogen bonds in transmembrane alpha-helices. Biophys. J. 2002; 83:2084–2095. [PubMed: 12324426]
57. Page RC, et al. Transmembrane helix uniformity examined by spectral mapping of torsion angles. Structure. 2008; 16:787–797. [PubMed: 18462683]
58. Dawson JP, et al. Motifs of serine and threonine can drive association of transmembrane helices. J Mol Biol. 2002; 316:799–805. [PubMed: 11866532]
59. Hall SE, et al. Position of helical kinks in membrane protein crystal structures and the accuracy of computational prediction. J. Mol. Graphics Modell. 2009; 27:944–950.
60. Zhou HX, McCammon JA. The gates of ion channels and enzymes. Trends Biochem. Sci. 2010; 35:179–185. [PubMed: 19926290]
61. Grigorieff N, et al. Lipid location in deoxycholate-treated purple membrane at 2.6 A. J Mol Biol. 1995; 254:404–415. [PubMed: 7490759]
62. Zhang H, et al. A defined protein-detergent-lipid complex for crystallization of integral membrane proteins: The cytochrome b6f complex of oxygenic photosynthesis. Proc Natl Acad Sci U S A. 2003; 100:5160–5163. [PubMed: 12702760]
63. Guan L, et al. Structural determination of wild-type lactose permease. Proc Natl Acad Sci U S A. 2007; 104:15294–15298. [PubMed: 17881559]
64. Cherezov V, et al. In meso structure of the cobalamin transporter, BtuB, at 1.95 A resolution. J. Mol. Biol. 2006; 364:716–734. [PubMed: 17028020]
65. Baker M. Structural biology: The gatekeepers revealed. Nature. 465:823–826. [PubMed: 20535212]
66. Cherezov V, et al. High-resolution crystal structure of an engineered human beta2-adrenergic G protein-coupled receptor. Science. 2007; 318:1258–1265. [PubMed: 17962520]
67. Hanson MA, et al. A specific cholesterol binding site is established by the 2.8 A structure of the human beta2-adrenergic receptor. Structure. 2008; 16:897–905. [PubMed: 18547522]
68. Liang B, et al. Fast-time scale dynamics of outer membrane protein A by extended model-free analysis of NMR relaxation data. Biochim. Biophys. Acta. 2010; 1798:68–76. [PubMed: 19665446]
69. Bocharov EV, et al. Spatial structure and pH-dependent conformational diversity of dimeric transmembrane domain of the receptor tyrosine kinase EphA1. J Biol Chem. 2008; 283:29385–29395. [PubMed: 18728013]
70. Lau TL, et al. Structure of the Integrin beta3 Transmembrane Segment in Phospholipid Bicelles and Detergent Micelles. Biochemistry. 2008; 47:4008–4016. [PubMed: 18321071]
71. Engelman DM. Membranes are more mosaic than fluid. Nature. 2005; 438:578–580. [PubMed: 16319876]
72. De Almeida RF, et al. Sphingomyelin/phosphatidylcholine/cholesterol phase diagram: boundaries and composition of lipid rafts. Biophys. J. 2003; 85:2406–2416. [PubMed: 14507704]
73. Cherezov V, et al. Membrane protein crystallization in meso: lipid type-tailoring of the cubic phase. Biophys. J. 2002; 83:3393–3407. [PubMed: 12496106]
74. Cantor RS. Lipid composition and the lateral pressure profile in bilayers. Biophys. J. 1999; 76:2625–2639. [PubMed: 10233077]
75. White SH, von Heijne G. How translocons select transmembrane helices. Annu. Rev. Biophys. 2008; 37:23–42. [PubMed: 18573071]

76. Yi M, et al. Test of the Gouy-Chapman theory for a charged lipid membrane against explicit-solvent molecular dynamics simulations. Phys. Rev. Lett. 2008; 101:038103. [PubMed: 18764300]

77. Nymeyer H, Zhou HX. A method to determine dielectric constants in nonhomogeneous systems: Application to biological membranes. Biophys. J. 2008; 94:1185–1193. [PubMed: 17951302]

78. Smart OS, et al. HOLE: a program for the analysis of the pore dimensions of ion channel structural models. J. Mol. Graph. 1996; 14:354–360. [PubMed: 9195488]

79. Page RC, et al. Lipid bilayers: an essential environment for the understanding of membrane proteins. Magn Reson Chem. 2007; 45:S2–S11. [PubMed: 18095258]

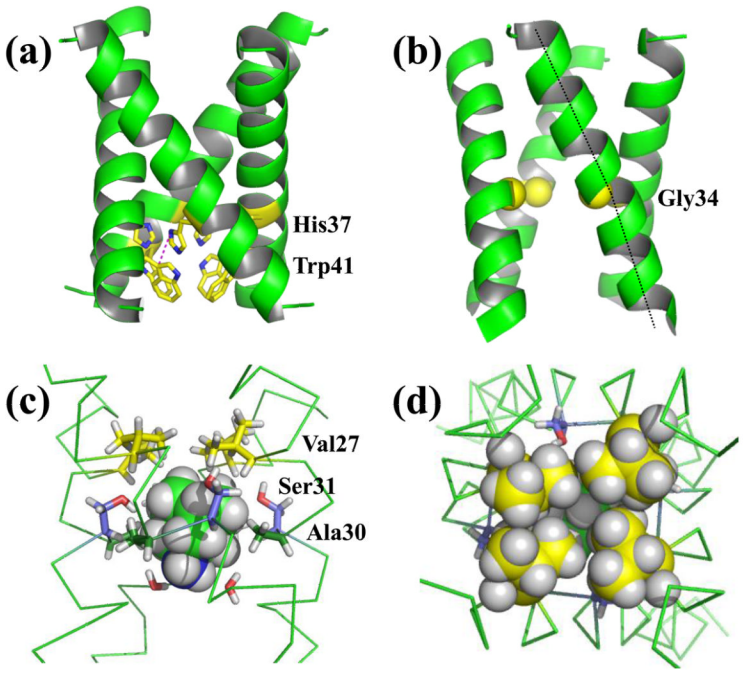

Figure 1.

Solid-state NMR structures of the M2 TM domain in liquid crystalline lipid bilayers. (**a**) Structure in the absence of amantadine (PDB entry 1NYJ). The observed short distance between His37 $N_{\delta 1}$ and Trp41 C_{γ} is indicated by a red dashed line. (**b**) Structure in the presence of amantadine (PDB entry 2H95). Note that the helices are kinked in the vicinity of Gly34 (shown as spheres); dashed lines are drawn through the N-terminal and C-terminal halves of one helix to highlight the kink. (**c**) The amantadine binding site, obtained from molecular dynamics simulations starting from 2H95. The bound amantadine (in space-filling representation) is located below the Val27 (yellow carbons) secondary gate and flanked by Ser31 (blue carbons) and Ala30 (dark green carbons) residues. Two waters that hydrogen bond to the downward-pointing amine are also shown. (**d**) The structure in (**c**) viewed from the viral exterior, with Val27 in space-filling representation showing that the secondary gate is closed.

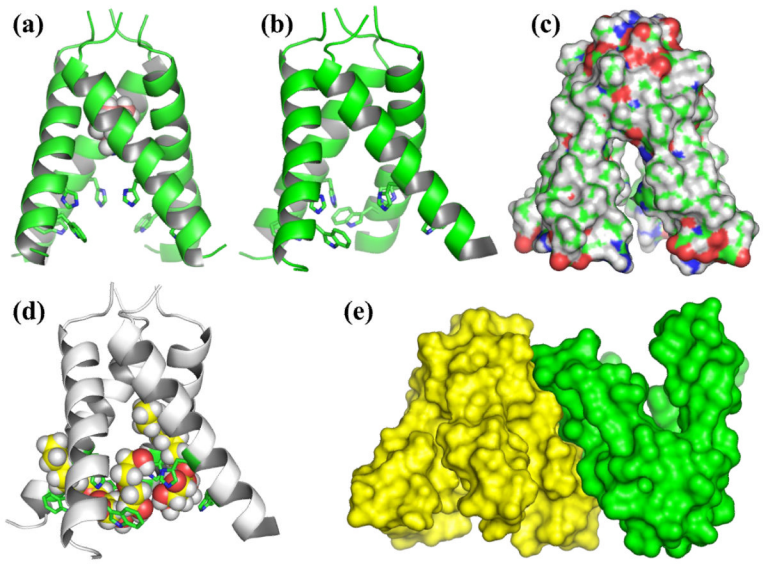

Figure 2.

Crystal structures of the M2 TM domain from octylglucoside solutions. (**a**) Structure of the amantadine-bound G34A mutant at pH 5.3 (PDB entry 3C9J). The bound amantadine is shown in space filling representation. (**b**)-(**e**) Different views of the TM domain determined at neutral pH (PDB entry 3BKD). In (**b**), the helical structure and even the His37 and Trp41 sidechains have nearly the same conformations as in the lowpH form shown in (**a**), except here one of the helices is significantly kinked near Gly34. (**c**) Surface rendering showing that the helices splay apart from the middle of the membrane toward the C-terminal end. (**d**) Similar orientation as in (**b**) but showing two octylglucoside and a polyethylene glycol molecule inserted into the tetrameric structure. (**e**) Surface rendering showing the crystal contacts between two tetramers in a unit cell.

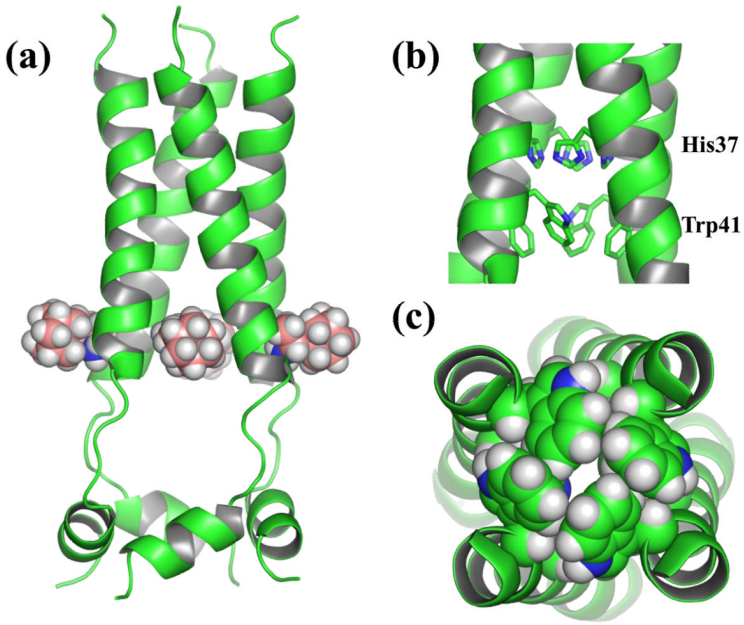

Figure 3.

Solution NMR structure of the M2 conductance domain determined in DHPC micelles (PDB entry 2RLF). (**a**) Overview of the NMR structure as a pair of four-helix bundles, one for the TM domain and one for the amphipathic helices C-terminal to the TM domain. Four rimantadine molecules (in space-filling representation) were bound to exterior of the TM helix bundle. The amphipathic helix bundle was found to be water soluble. (**b**) and (**c**) Two views of the HxxxW quartet in the NMR structure. In (**b**) a side view is shown. In (**c**) a view from the viral interior illustrates the tight packing of the Trp41 sidechains (in space-filling representation) and as such their inability to serve as a gate.

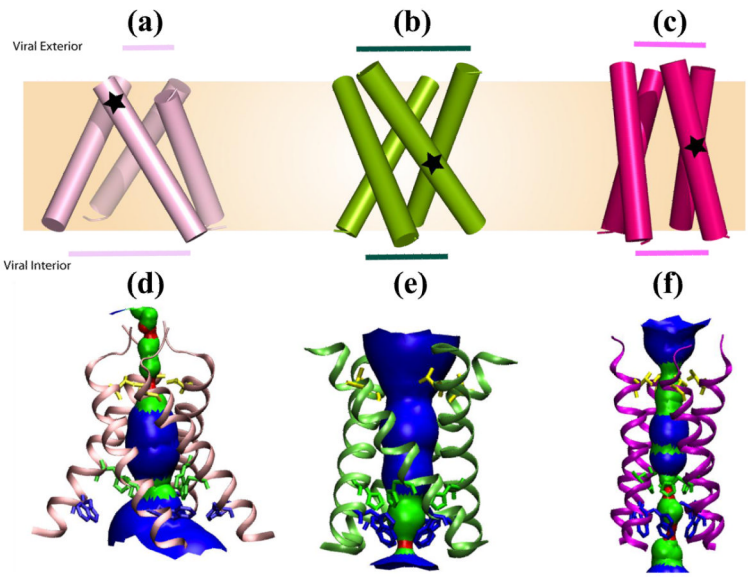

Figure 4.

Comparison of TM helix packing in three neutral-pH M2 structures, illustrating the influence of solubilizing environments. (**a**) X-ray structure crystallized from octylglucoside solutions (PDB entry 3BKD). (**b**) Solid-state NMR structure determined in liquid crystalline lipid bilayers (PDB entry 1NYJ). (**c**) Solution NMR structure determined in DHPC micelles (PDB entry 2RLF). Colored bars above and below the structures indicate the separation of the helices on either side of the membrane; stars indicate helix crossing points. (**d**)-(**f**) "HOLE" images [78] for the structures in (**a**)-(**c**) displaying the variations of the channel pore due to different helix packing. Pore size color code: red (< 1.2 Å, radius of a water molecule); green (< 3 Å, radius of amantadine); and blue (> 3 Å).